Thin and temperature resistant TiO2-Sr1-xLaxTiO3 (x=0.1~0.3) composite ceramics for microwave absorption in the X-band

Yingying Zhou (zhouyingying@xaau.edu.cn)
Xi'an Aeronautical University https://orcid.org/0000-0002-7872-6894
Qinlong Wen
Northwestern Polytechnical University
Chaoqun Yang
Xi'an Aeronautical University
Zhaowen Ren
Northwestern Polytechnical University
Yuanyuan Lu
Xi'an Aeronautical University
Youquan Wan
Xi'an Aeronautical University
Dan Chen
Xi'an Aeronautical University
Hui Xie
Xi'an Aeronautical University

Research Article

Keywords: Strontium titanate, La doping, Dielectric, Microwave absorbing

Posted Date: February 25th, 2021

DOI: https://doi.org/10.21203/rs.3.rs-240947/v1

Version of Record: A version of this preprint was published at Journal of Materials Science: Materials in Electronics on April 1st, 2021. See the published version at https://doi.org/10.1007/s10854-021-05798-6.

Thin and temperature resistant TiO_2-$Sr_{1-x}La_xTiO_3$ (x=0.1~0.3) composite ceramics for microwave absorption in the X-band

Yingying Zhou[1, 2*], Qinlong Wen[1], Chaoqun Yang[1], Zhaowen Ren[2], Yuanyuan Lu[1], Youquan Wan[1], Dan Chen[1], Hui Xie[1]

1. School of Materials Engineering, Xi'an Aeronautical University, Xi'an 710077, P.R. China;

2. State Key Laboratory of Solidification Processing, School of Materials Science and Engineering, Northwestern Polytechnical University, Xi'an 710072, P.R. China;

*corresponding author: zyzlchappy1989@163.com

Abstract

Recently, high-temperature stability is a challenge in a number of microwave absorption materials. Hence, researchers are still searching for a novel material system preferably with a high-temperature resistance to be applied in the field of microwave absorption. Here, in the current study, toward this aim, lanthanum (La) doped strontium titanate ($SrTiO_3$) blended with TiO_2 were fabricated by hot-press sintering in vacuum. The as-prepared samples are denoted as TiO_2-$Sr_{1-x}La_xTiO_3$ with x varying from 0.1 to 0.3 in steps of 0.1. Scanning electron microscope (SEM), X-ray diffraction (XRD), X-ray photoelectron spectroscope (XPS), and microwave vector network analyzer were carried on to study their morphology, phase composition, structure, electromagnetic and microwave absorption properties, respectively. It is revealed that the La atom was efficiently doped at the Sr-site in $SrTiO_3$. Benefiting from the tunability of its dielectric and impedance properties, TiO_2-$Sr_{1-x}La_xTiO_3$ can be utilized in a highly efficient way to absorb microwave radiations with a decent design. Results illustrated that TiO_2-$Sr_{1-x}La_xTiO_3$ (x=0.2) with a thickness of only 0.42 mm exhibits a high microwave absorption efficiency of -40.89 dB and can achieve a 2.82 GHz bandwidth of reflection loss value below -5 dB. Thus, TiO_2-$Sr_{1-x}La_xTiO_3$ composites ceramics can be served as an opening opportunity for the application of high-temperature stability and tunable high-performance effectiveness microwave absorption materials in stealth technology and information security.

Keywords: Strontium titanate; La doping; Dielectric; Microwave absorbing

1. Introduction

Along with the fast and fierce evolution of civil network technology and military detection technology, the protection or absorption technology of electromagnetic (EM) wave radiation is becoming of increasing significance in this day and age [1]. In order to address this issue, microwave absorbing materials (MAMs) are increasingly being studied for their isolating and absorbing the EM wave from the surroundings. At present, in addition to the conventional requirements for MAMs: thin thickness, lightweight, wide absorption band, strong absorption capacity, a fifth requirement has been put forward, i.e., high-temperature resistance. It is well known that meeting these five performance requirements simultaneously can be extremely challenging [2]. Currently, one most commonly used MAMs is ferromagnetic materials-based absorbing materials [3, 4] or carbon-based absorbing materials [5, 6], which can absorb or attenuate EM waves using magnetic or electrical losses. However, they are susceptible to high-temperature oxidation, chemical corrosion, or heavyweight, which dramatically limits their applications in the field of microwave absorption.

Perovskite structure oxide, ABO_3, has been largely investigated due to properties related to their versatile dielectric, ferroelectric, and spontaneous polarization [7, 8]. Among such materials, $SrTiO_3$ with cubic symmetry (Pm3m) perovskite structure, high chemical, and thermal stability has been applied comprehensively in electronic, energy storage, and ceramic industries. However, owing to its nonmagnetic loss ($\tan \mu$) and low dielectric loss ($\tan \delta$), it is almost impossible for untreated or modified or pure $SrTiO_3$ to be employed as MAM. The nonabsorbent state related to electric and dielectric properties of $SrTiO_3$, however, can be altered by chemical substitutions [9]. For instance, the A-site substitution of Sr^{2+} by nonisovalent (e.g., Gd^{3+}, La^{3+}, etc.) polar impurities, $SrTiO_3$ can be transformed into an n-type electric state. On the one hand, it is ascribed to the existence of defects, including oxygen vacancies, polar nanoregions, and defect centers caused by charge imbalance between the substituted ion and the replaced ion [10]. On the other hand, it is attributed to the structural defects created by ionic radius mismatch between host and dopant cations resulting in elastic lattice strains and leading to the polar states [8]. Therefore, doped $SrTiO_3$ is of great potential as MAMs with excellent comprehensive performance especially high-temperature resistance for low-cost and sustainable materials resources. However, there are scarce studies on the microwave absorption performance of doped

$SrTiO_3$. Clearly, there remains a need for systematic research on the impact of substitution ions and amounts on the microwave absorption properties of $SrTiO_3$. Therefore, in this study, $Sr_{1-x}La_xTiO_3$ ceramics synthesized using La^{3+} donor with a higher valence than the host Sr^{2+} ion as a dopant for the Sr-site in $SrTiO_3$. La was chosen as the dopant mainly for two reasons. One reason is that La is well known for being substituted exclusively at the Sr site as La^{3+} [11-14]. The second reason is that $SrTiO_3$'s electrical properties can be significantly modified even when the amount of La doping content is tiny [15-17].

In view of the foregoing discussion, composite ceramics composed of $Sr_{1-x}La_xTiO_3$ as absorbers and TiO_2 as matrix were fabricated using a hot-press sintering process in a vacuum atmosphere. The influence of different La doping concentrations on the microstructure, morphology, dielectric, and microwave absorption properties in X-band were systematically studied.

2. Materials and Methods

Specimens were prepared by the conventional mixed oxide method using strontium carbonate ($SrCO_3$, AR), lanthanum (III) oxide (La_2O_3, 99.99%), and titanium dioxide (TiO_2, CP) as raw materials, which were purchased from Sinopharm Chemical Reagent Co., Ltd. Firstly, appropriate amounts of $SrCO_3$, La_2O_3, and TiO_2 were ball-milled for 12 h using ZrO_2 balls in alcohol, followed by drying at 100 °C in an oven for several hours. Then the mixing powders were sintered at 1250 °C for 2 h in the air atmosphere to prepare $Sr_{1-x}La_xTiO_3$. Subsequently, the calcined $Sr_{1-x}La_xTiO_3$ and TiO_2 powders were blended in a proportion of 75:25 and pressed into disk samples of φ = 35 mm, followed by calcining at 1300 °C for 2 h by a hot-press sintering system in a vacuum atmosphere.

The morphologies and microstructures of these as-fabricated specimens were investigated by scanning electron microscope (SEM, VEGA3, TESCAN, Czech Republic). The crystal phase compositions of the synthesized specimens were characterized by X-ray diffraction (XRD, X'Pert PRO, PANalytical, the Netherlands) in the 2θ range from 10° to 90° with CuKα radiation. X-ray photoelectron spectroscope (XPS, ULVAC-PHI Versa-probe) using a monochromated Al Kα excitation source was conducted to determine surface composition of the TiO_2-$Sr_{1-x}La_xTiO_3$ ceramics. The obtained ceramics were cut into rectangular bars (22.86×10.16×1.50 mm), and the electromagnetic parameters were measured using a

two-port microwave vector network analyzer (VNA, N5225B, Keysight Technologies, USA) in the X band (frequency range: 8.2~12.4 GHz). The microwave reflection loss (RL) value, which reflects the microwave absorption performance, was calculated based on transmission line theory.

3. Result and discussion

3.1 Morphology analysis

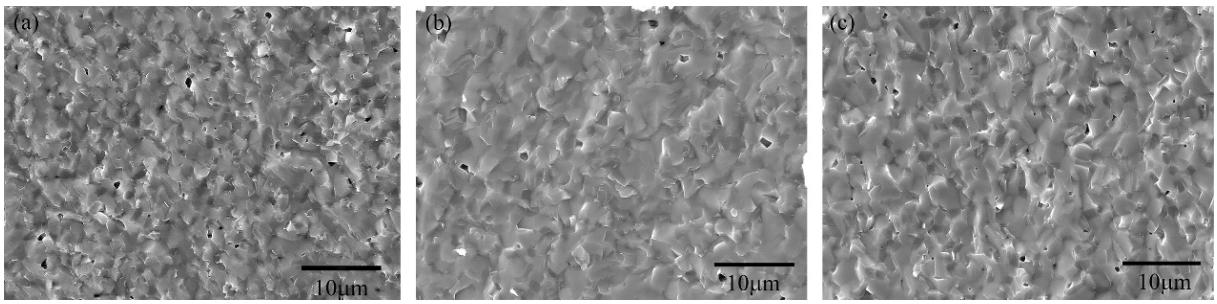

Fig. 1 SEM images of the fracture cross-section morphologies of TiO_2-$Sr_{1-x}La_xTiO_3$: (a) x=0.1, (b) x=0.2, (c) x=0.3.

Figure 1 exhibits the secondary electron SEM images of the cross-section of TiO_2-$Sr_{1-x}La_xTiO_3$ ceramics with different La doping concentrations. As revealed in Fig. 1, all the samples with different La doping concentrations (x=0.1~0.3) possess similar microstructure and porosity on the scale of size and degree. There are only a small number of pores in these three ceramics, indicating a dense microstructure was formed after the hot-pressing process. Moreover, the grain size increases on the whole with increasing La doping contents, which may be because the substitution of La is beneficial in promoting the grain growth [18, 19].

3.2 Phase composition analysis

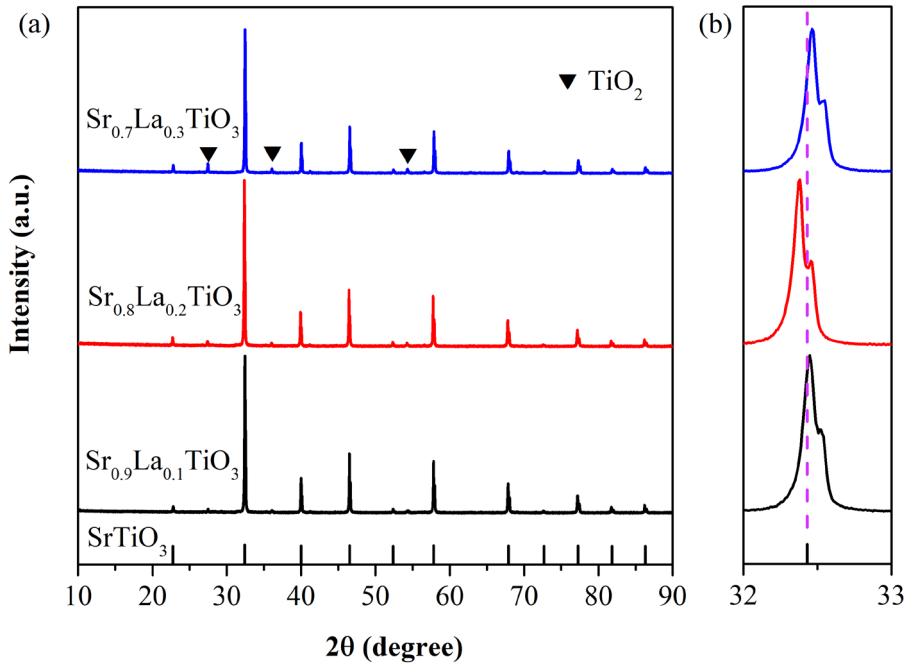

Fig. 2 XRD diffraction patterns of TiO_2-$Sr_{1-x}La_xTiO_3$: (a) whole patterns; (b) magnification peak distributed from 32° to 33°.

To reveal the influence of La doping on the crystal structure, the XRD diffraction experiments with different La doping concentrations were carried out, as displayed in Fig. 2. As shown in Fig. 2a, two main phases were present in the XRD patterns of the TiO_2-$Sr_{1-x}La_xTiO_3$ ceramics that could be assigned to the reflections of $SrTiO_3$(JCPDS card No. 89-4934)) and TiO_2(JCPDS card No. 21-1276). Furthermore, it indicates that the XRD diffraction pattern of $Sr_{1-x}La_xTiO_3$ is highly consistent with the standard card of $SrTiO_3$ to a certain degree. It demonstrates that the crystal structure of $SrTiO_3$ does not change as La-doped in such concentrations (x=0.1~0.3). Fig. 2b shows one of the diffraction spectra of $Sr_{1-x}La_xTiO_3$ from 32° to 33°correspond to (110) plane of $SrTiO_3$. It can be discovered that the peak position of $Sr_{1-x}La_xTiO_3$ slightly shifted toward a lower 2θ value and then tended to have a higher 2θ value with increasing x value. According to the Bragg spacing equation $2d\sin\theta=n\lambda$ [20], the interplanar spacing $d_{(110)}$ of $Sr_{1-x}La_xTiO_3$ first increases and subsequently decreases with the raising of x value. Incorporating a certain concentration of La, the lattice parameters of SrTiO3 can be affected by two mechanisms. One noticeable mechanism is caused by the atom size mismatch among the dopant atom La and the host atom Sr. The other mechanism is electronic effects [21]. Because of the smaller ion radius La^{3+} (1.36 Å, coordination number CN=12) [22] substituting for the larger ion radius Sr^{2+} (1.44 Å, CN=12) [23], as to the first mechanism, the interplanar spacing d of $Sr_{1-x}La_xTiO_3$ should be reduced

as La doping contents increases. However, on the other hand, with La^{3+} as a donor impurity doping in Sr^{2+} of $SrTiO_3$ lattice, a considerable proportion of electrons were placed in the conduction band. The system would reduce its energy by lowering the conduction band's position, accompanied by volume deformations, which is described through deformation potential [21]. Consequently, under the influence of deformation potential, the interplanar spacing *d* of $Sr_{1-x}La_xTiO_3$ increases with the doping of La. Accordingly, combining size effect and deformation potential effect, the deformation potential effect dominates first, whereas the size effect predominates later.

3.3 XPS analysis

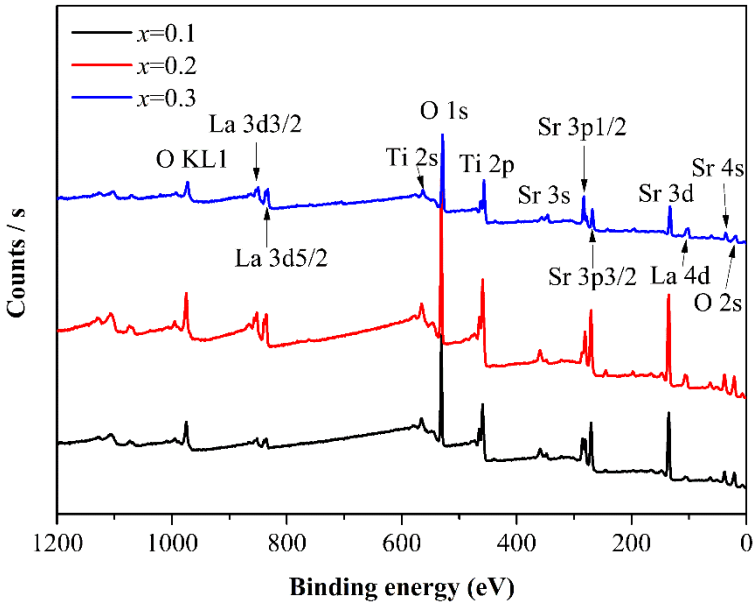

Fig. 3 A wide survey scan XPS spectra of TiO_2-$Sr_{1-x}La_xTiO_3$.

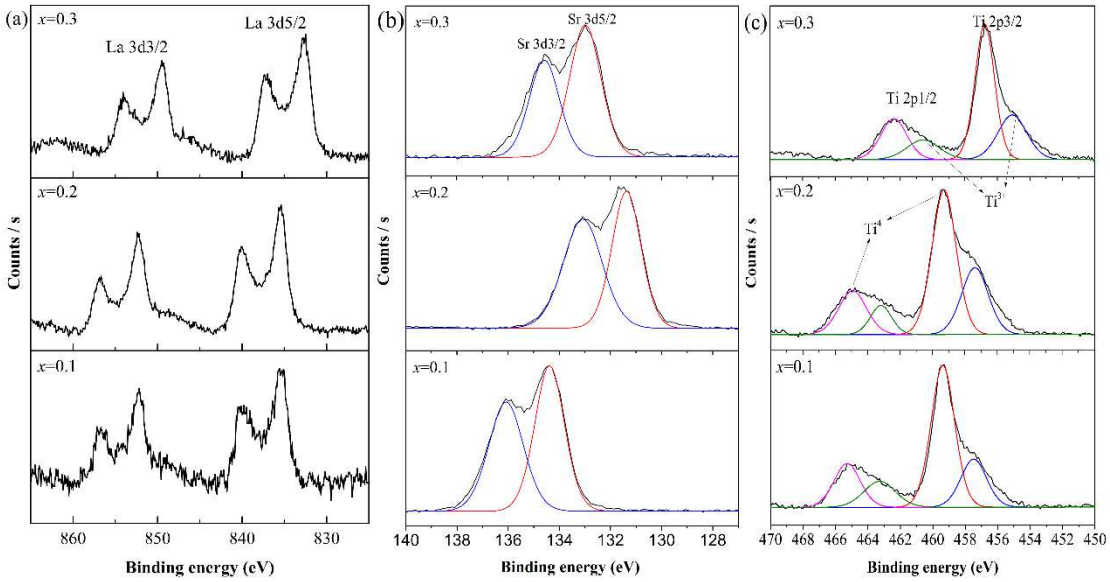

Fig. 4 High-resolution XPS spectra of TiO_2-$Sr_{1-x}La_xTiO_3$ ceramics in (a) La, (b) Sr and (c) Ti.

Here XPS test was executed to investigate the chemical states of TiO_2-$Sr_{1-x}La_xTiO_3$. The XPS measurement scan was conducted from 0 eV to 1200 eV binding energy, which covers the core levels of all elements of Sr, La, Ti, and O, as shown in Fig. 3. It confirms the presence of La in all the TiO_2-$Sr_{1-x}La_xTiO_3$ ceramics, demonstrating that La successfully substituted Sr site in $SrTiO_3$. Figure 4 presents the high-resolution XPS spectra of TiO_2-$Sr_{1-x}La_xTiO_3$, which belongs to the oxidation states of La, Sr, and Ti. As shown in Fig. 4a, the binding energy positions of La $3d_{3/2}$ and La $3d_{5/2}$ correspond to the oxidation states of La^{3+} [24]. It can also be observed from Fig. 4 that the binding energy of La first increases slightly and then decreases. It can be attributed to the changes in the relative number of electrons in the outer layer of La due to the twisted structures and changed cell size of $Sr_{1-x}La_xTiO_3$. The core level spectrum of Sr $3d$ displays the doublet peaks for Sr $3d_{5/2}$ and Sr $3d_{3/2}$, confirming the Sr^{2+} state in the sample (Fig. 4b) [25]. The binding energy shift of Sr is opposite to that of La. The XPS spectra of Ti (Fig. 4c) exhibit two distinct broad peaks of Ti $2p_{3/2}$ and Ti $2p_{1/2}$ are corresponding to the combination of Ti^{4+} and Ti^{3+} in the perovskite structure of $Sr_{1-x}La_xTiO_3$, which can be attributed to the La^{3+} doping [26, 27].

3.4 Dielectric properties

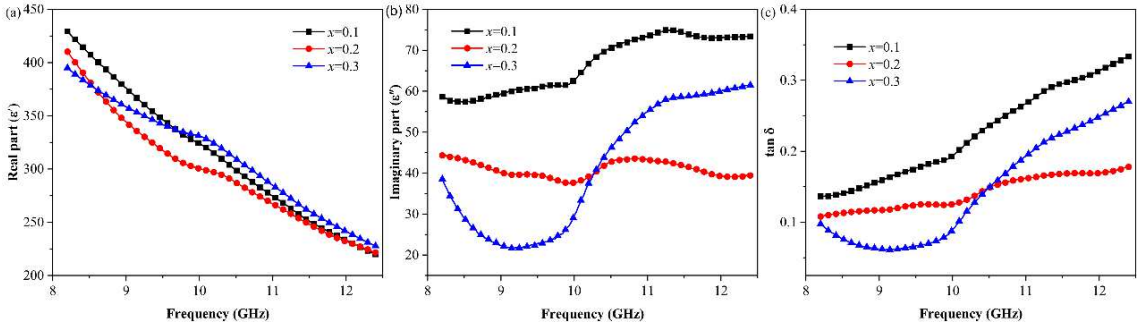

Fig. 5. Dielectric parameters of (a) the real part, (b) the imaginary part, and (c) the dielectric loss for TiO_2-$Sr_{1-x}La_xTiO_3$ ceramics.

It is well acknowledged that the dielectric permittivity is of the essence to nonmagnetic microwave absorbing materials. Thus, the dielectric permittivity

parameters were measured in the X band. Dielectric parameters of the real part of dielectric permittivity (ε'), the imaginary part of dielectric permittivity (ε''), and dielectric loss (tan δ) for TiO_2-$Sr_{1-x}La_xTiO_3$ (x=0.1~0.3) ceramics are shown in Fig. 5. It can be noted from Fig. 5a that the real part of all the three samples displays good frequency dispersion relation, i.e., their values decrease rapidly with the increasing frequency, which is beneficial to broaden the absorption band. Furthermore, the ε' value of TiO_2-$Sr_{0.8}La_{0.2}TiO_3$ shows lower on the whole than the other two dopants, indicating that the primary reflection of the microwave is weak, which is conducive to impedance matching [28].

Figure 5b shows the imaginary part of dielectric permittivity of TiO_2-$Sr_{1-x}La_xTiO_3$ with three doping contents (x=0.1~0.3). According to the Debey theory, ε'' can be determined as follows [29].

$$\varepsilon'' = \frac{(\varepsilon_s - \varepsilon_\infty)\omega\tau}{1+\omega^2\tau^2} + \frac{\sigma}{\omega\varepsilon_0} \quad (1)$$

where ε_∞, ε_s, and ε_0 is the high-frequency limit permittivity, static permittivity, and free space permittivity, respectively. ω is the angular frequency, and $\omega=2\pi f$. τ is the relaxation time and σ is the electrical conductivity of the as-prepared ceramics. The first item in Eq. (1) is the loss related to the Maxwell-Wagner-Sillars (MWS) polarization process. This function depends on the electric dipole's charge, and its value is strongly dependent on the microwave energy dissipation originated from the reorientation of electric dipoles. The last item is associated with conductance loss resulting from the movement of charge carriers such as electronic and ionic. Furthermore, due to the minimal number of electronics in such ceramics we researched, the electron conductance loss can be ignored. In contrast, the loss of ionic conductivity, including intrinsic ionic conductivity and impurity ionic conductivity, plays an important role. The intrinsic ionic conductance loss is the energy loss caused by the current formed by the directional movement of defects (including Schottky defects and Frenkel defects) along the electric field's direction after being excited by the external electric/magnetic field and heat. The impurity ionic defect complexes can be depicted in Eq. (2), where the Kröger-Vink defect symbol [30] was used.

$$La_2O_3 \xrightarrow{SrTiO_3} La_{Sr}^{\bullet} + La_i^{\bullet\bullet\bullet} + V_{Ti}^{\prime\prime\prime\prime} + 3O_o^{\times} \quad (2)$$

where " • ", " ′ " and " × " represent the defect is positively charged, negatively charged, and neutral, respectively. The defect reaction equilibrium equation is built based on the principle of particle positions, charge equilibrium, and mass equilibrium. After La doping in $SrTiO_3$, defects such as $La_{Sr}^{\bullet}$, $La_i^{\bullet\bullet\bullet}$, and $V_{Ti}^{\prime\prime\prime\prime}$ with the ability to transmit electrons were created that will consume plenty of energy. Fig. 5c displays the dielectric loss of TiO_2-$Sr_{1-x}La_xTiO_3$ (x=0.1~0.3) ceramics. It indicates the sample of x=0.1 possesses the highest dielectric loss compared with the other samples, consistent with the variety imaginary part of dielectric (Fig. 5b).

3.5 Microwave absorption properties

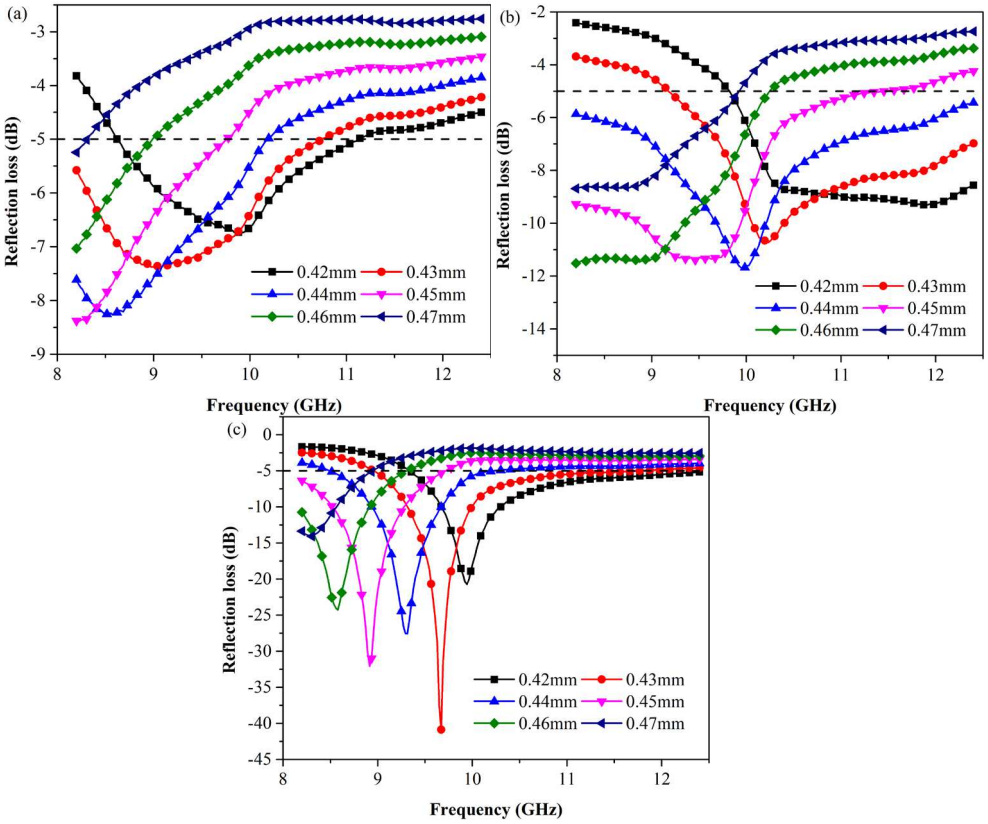

Fig. 6. Reflection loss of (a) TiO_2-$Sr_{0.9}La_{0.1}TiO_3$, (b) TiO_2-$Sr_{0.8}La_{0.2}TiO_3$, and (c) TiO_2-$Sr_{0.7}La_{0.3}TiO_3$ with different thicknesses.

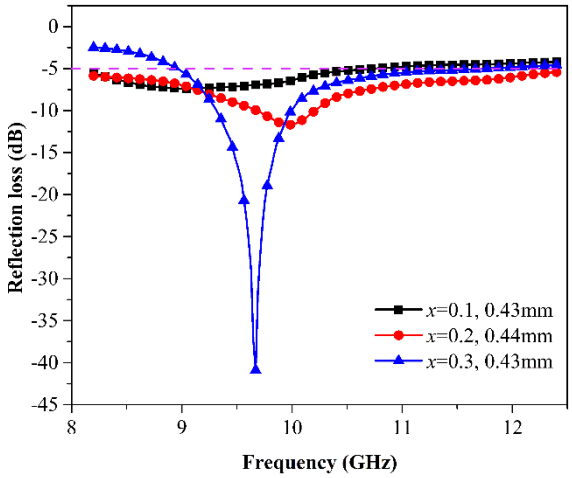

Fig. 7. Comparison of reflection loss value of TiO_2-$Sr_{1-x}La_xTiO_3$ (x=0.1~0.3) ceramics with optimum thicknesses.

To further evaluate the overall electromagnetic wave absorbing performance of the TiO_2-$Sr_{1-x}La_xTiO_3$ (x=0.1~0.3) ceramics, the reflection loss (RL) value was computed by the following equations based on data from 3.4 part.

$$\mathrm{RL(dB)} = 20\lg\left|\frac{Z_{in}-1}{Z_{in}+1}\right| \tag{3}$$

$$Z_{in} = \sqrt{\frac{\mu_r}{\varepsilon_r}}\tanh\left(j\frac{2\pi f d}{c}\sqrt{\mu_r\varepsilon_r}\right) \tag{4}$$

where RL is the reflection loss in dB unit, Z_{in} is the input impedance of absorber, ε_r and μ_r are, respectively, the complex permittivity and permeability, $j = \sqrt{-1}$ is the imaginary unit, f is the frequency of the incident electromagnetic wave, d is the thickness of the absorber, c is the velocity of light. It is worth mentioning that μ_r=1 for nonmagnetic material, and all the materials prepared in this paper are nonmagnetic. Generally, it was proven that an absorber with excellent electromagnetic wave absorbing performance results from good impedance matching and high energy dissipation capability.

The electromagnetic wave absorption performance of the TiO_2-$Sr_{1-x}La_xTiO_3$ (x=0.1~0.3) ceramics with different thicknesses (0.42~0.47 mm) can be gained using Eqs. (3) and (4), as displayed in Fig. 6. On the whole, Fig. 6 illustrates that TiO_2-$Sr_{1-x}La_xTiO_3$ (x=0.1~0.3) ceramics behave very different absorption performance at different x values (i.e., different La doping contents) in the same thickness range. It suggests La doping concentration directly reflects the electromagnetic wave absorption performance of TiO_2-$Sr_{1-x}La_xTiO_3$ ceramics. In purpose to further study the absorption results of TiO_2-$Sr_{1-x}La_xTiO_3$, the effective bandwidth of RL$\leqslant$-5 dB (RL_{-5})

and minimum RL (RL_{min}) value equivalent to the maximum absorption, which can be identified in Fig. 6, were indicated in Table 1. It can be seen that among the as-prepared samples, the widest absorption band is 4.2 GHz, which appears in the TiO_2-$Sr_{0.8}La_{0.2}TiO_3$ ceramic. Consequently, when the content of La was 0.2 at.% (x=0.2), TiO_2-$Sr_{1-x}La_xTiO_3$ ceramic possesses better absorption performance in terms of bandwidth within the test frequency band. The minimum absorption peak appeared in TiO_2-$Sr_{0.7}La_{0.3}TiO_3$ ceramic with a thickness of 0.43 mm, and the RL_{min} is -40.89 dB. Therefore, from the point of view of RL_{min}, among the samples, TiO_2-$Sr_{0.7}La_{0.3}TiO_3$ shows the best absorbing performance.

Figure 7 exhibits the comparison of RL value of TiO_2-$Sr_{1-x}La_xTiO_3$ (x=0.1~0.3) ceramics with optimum thicknesses (0.43~0.44 mm). As shown in Fig. 7, with the gain of La doping concentration, the RL_{min} value is promoted and the maximum RL_{min} value reached -40.89 dB when the doping concentration of La is x = 0.3. However, the effective absorption bandwidths have been proved to be a substantial factor in engineering applications [31]. Therefore, on the one hand, the TiO_2-$Sr_{0.8}La_{0.2}TiO_3$ ceramic with a thickness of only 0.44 mm owns an outstanding microwave absorption performance with a maximum absorption peak of -11.7 dB and bandwidth (RL_{-5}) of 4.2 GHz. On the other hand, TiO_2-$Sr_{0.7}La_{0.3}TiO_3$, with a thickness of only 0.43 mm, holds a maximum absorbing peak of -40.89 dB and bandwidth (RL_{-10}) of 0.67 GHz, belongs to one of the best candidates of electromagnetic wave absorption materials among materials prepared in this work. As demonstrated above, TiO_2-$Sr_{1-x}La_xTiO_3$ ceramics can be used as good candidate microwave absorbing materials at X band by modifying La doping contents.

Table 1 The detailed microwave absorption performance of TiO_2-$Sr_{1-x}La_xTiO_3$ (x=0.1~0.3) ceramics

x value	Thickness (mm)	RL_{min} (dB)	Bandwidth of RL≤-5 dB (GHz)	Band range (GHz)
0.1	0.42	-6.48	2.54	8.62~11.16
	0.43	-7.40	2.56	8.2~10.76
	0.44	-8.26	2	8.2~10.2
	0.45	-8.39	1.55	8.2~9.75
	0.46	-7.03	0.78	8.2~8.98
	0.47	-5.24	0.11	8.2~8.31

0.2	0.42	-9.33	2.6	9.8~12.4
	0.43	-10.72	3.22	9.18~12.4
	0.44	-11.70	4.2	8.2~12.4
	0.45	-11.39	3.3	8.2~11.5
	0.46	-11.52	2.04	8.2~10.24
	0.47	-8.69	1.72	8.2~9.92
0.3	0.42	-20.73	3.06	9.34~12.4
	0.43	-40.89	2.82	8.97~11.79
	0.44	-27.55	1.73	8.49~10.22
	0.45	-32.07	1.51	8.2~9.71
	0.46	-24.27	1.11	8.2~9.31
	0.47	-14.11	0.74	8.2~8.94

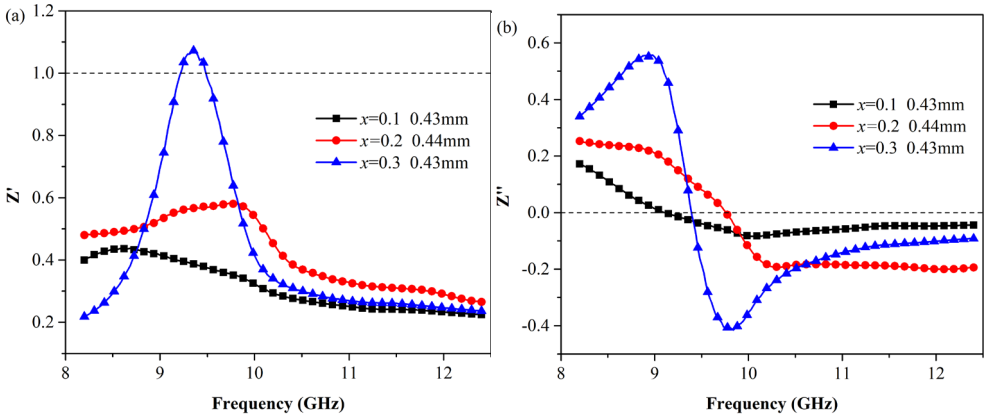

Fig. 8. Plots of (a) real and (b) imaginary parts of impedance of TiO_2-$Sr_{1-x}La_xTiO_3$ with optimum thicknesses.

The real part *Z*' and imaginary part *Z*'' of the complex impedance was calculated with the corresponding thickness for optimum absorption performance. The variation of *Z*' and *Z*'' vs. frequency plot of TiO_2-$Sr_{1-x}La_xTiO_3$ (x=0.1~0.3) ceramics is displayed in Fig. 8. It can be seen that the curves are frequency-dependent and both the *Z*' and *Z*'' curves show significant differences with different amounts of La doping. The large fluctuation of TiO_2-$Sr_{0.7}La_{0.3}TiO_3$ in *Z*' and *Z*'' curves is associated with the complex permittivity fluctuation (Fig. 5). It also can be seen that samples with x=0.2 and 0.3 achieve good impedance matching, resulting in quite good electromagnetic wave transmission [32].

4. Conclusions

In summary, TiO_2-$Sr_{1-x}La_xTiO_3$ ceramics with dense microstructure were fabricated by hot-press sintering process in a vacuum. It has been indicated that, after the introduction of La ion, the lattice parameter and crystallographic structure of $SrTiO_3$ were affected by both deformation potential and size effect. Benefiting from MWS polarization process and conductance loss, all the as-prepared TiO_2-$Sr_{1-x}La_xTiO_3$ ceramics exhibited high dielectric loss. Not only the high dielectric loss, but also the good impedance resulted in the excellent wave absorbing properties of TiO_2-$Sr_{1-x}La_xTiO_3$ (x= 0.2 and 0.3). The minimum RL of TiO_2-$Sr_{0.7}La_{0.3}TiO_3$ can reach -40.89 dB with a thickness of only 0.43 mm. Therefore, the La doped TiO_2-$Sr_{1-x}La_xTiO_3$ composite ceramics with thin thickness are promising MAMs in X-band.

Acknowledgments

This work was financially supported by the National Natural Science Foundation of China (Grant No. 51701148), Natural Science Foundation of Shaanxi Province (Grant No. 2019JQ-916 and 2020JQ-912), Innovation and entrepreneurship training program for University Students (Grant No. S202011736018).

References

[1] K. Zhao, S. Gupta, C. Chang, J. Wei, N. H. Tai, RSC Adv. 9 19217-19225 (2019).

[2] Y. Zhou, L. Ma, R. Li, D. Chen, Y. Lu, Y. Cheng, X. Luo, H. Xie, W. Zhou, J. Magn. Magn. Mater. 524, 167681 (2021).

[3] X. Yang, Y. Duan, Y. Zeng, H. Pang, G. Ma, X. Dai, J. Mater. Chem. C 8, 1583-1590 (2020).

[4] H. Wei, Z. Zhang, G. Hussain, L. Zhou, Q. Li, K. Ostrikove, *Appl. Mater. Today* 19, 100596 (2020).

[5] X. Li, Y. Zhu, X. Liu, B.B. Xu, Q. Ni, Compos. Struct. 238, 111954 (2020).

[6] K. Pan, T. Leng, J. Song, C. Ji, J. Zhang, J. Li, K.S. Novoselov, Z. Hu, Carbon 160, 307-316 (2020).

[7] N. Pryds, V. Esposito, Metal oxide-based thin film structures, 1st edn. (Elsevier, 2018), pp. 465-488.

[8] L. Fang, W. Dong, F. Zheng, M. Shen, J. Appl. Phys. 112, 034114 (2012).

[9] H. Xie, C. Yang, Y. Zhou, Z. Ren, P. Liu, J. Mater. Sci- Mater El. 31, 16178-16188 (2020).

[10] X. Wang, Q. Hu, L. Li, X. Lu, J. Appl Phys. 112, 044106 (2012).

[11] C.D. Savaniu, J. T.S. Irvine, Solid State Ionics 192, 491-493 (2011).

[12] M. Qin, F. Gao, G. Dong, J. Xu, M. Fu, Y. Wang, M. Reece, H. Yan, J. Alloy. Compd. 762, 80-89 (2018).

[13] Z.Y. Shen, Q.G. Hu, Y.M. Li, Z.M. Wang, W.Q. Luo, Y. Hong, Z.X. Xie, R.H. Liao, J. Am. Ceram. Soc. 96, 2551-2555 (2013).

[14] H. Muta, K. Kurosaki, S. Yamanaka, J. Alloy. Compd. 368, 22-24 (2004).

[15] D. Liu, Y. Zhang, H. Kang, J. Li, Z. Chen, T. Wang, J. Eur. Ceram. Soc. 38, 807-811 (2018).

[16] J. Han, Q. Sun, Y. Song, J. Alloys Compd. 705, 22-27 (2017).

[17] D. Srivastava, C. Norman, F. Azough, M.C. Schäfer, E. Guilmeau, D. Kepaptsoglou, Q.M. Ramasse, G. Nicotra, R. Freer, Phys. Chem. Chem. Phys. 18, 26475-26486 (2016).

[18] M. Neuschitzer, J. Marquez, S. Giraldo, M. Dimitrievska, M. Placidi, I. Forbes, V. Izquierdo-Roca, A. Pérez-Rodriguez, E. Saucedo, J. Phys. Chem. C 120, 9661-9670 (2016).

[19] J. Chen, H. Lin, D. Hao, Y. Tang, X. Yi, Y. Zhao, S. Zhou, Scripta Mater. 162, 82-85 (2019).

[20] Q.L. Li, Y.F. Sun, Y.L. Sun, J.J. Wen, Y. Zhou, Q.M. Bing, L.D. Isaacs, Y.H. Jin, H. Gao, Y.W. Yang, Chem. Mater. 26, 6418-6431 (2014).

[21] A. Janotti, B. Jalan, S. Stemmer, C.G.V. Walle, Appl. Phys. Lett. 100, 262104 (2012).

[22] D.Y. Lu, Y. Yue, X.Y. Sun, J. Alloy. Compd. 586, 136-141 (2014).

[23] R.Y. Jing, X.M. Chen, H.L. Lian, X.S. Qiao, X.J. Shao, J.P. Zhou, J. Eur. Ceram. Soc. 38, 3111-3117 (2018).

[24] A.J. Ahmed, M.S.A. Hossain, S.M.K.N. Islam, F. Yun, G. Yang, R. Hossain, A. Khan, J. Na, M. Eguchi, Y. Yamauchi, X.L. Wang, ACS Appl. Mater. Interfaces 12, 28057-28064 (2020).

[25] M.E. Pilleux, C.R. Grahmann, V.M. Fuenzalida, J. Am. Ceram. Soc. 77, 1601-1604 (1994).

[26] M. Qin, F. Gao, G. Dong, J. Xu, M. Fu, Y. Wang, M. Reece, H. Yan, J. Alloy. Compd. 762, 80-89 (2018).

[27] D.Q. Liu, Y.W. Zhang, H.J. Kang, J.L. Li, X. Yang, T.M. Wang, Chinese Phys. B 27, 047205 (2018).

[28] H. Wei, X. Yin, Z. Hou, F. Jiang, H. Xu, M. Li, L. Zhang, L. Cheng, J. Eur. Ceram. Soc. 38, 4189-4197 (2018).

[29] Q. Wen, W. Zhou, H. Gao, Y. Zhou, F. Luo, D. Zhu, Z. Huang, Y. Qing, Appl. Phys. A-Mater. 125, 413 (2019).

[30] F.A. Kröger, H.J. Vink, Solid State Phys. 3, 307-435 (1956).

[31] Y. Qing, D. Min, Y. Zhou, F. Luo, W. Zhou, Carbon 86, 98-107 (2015).

[32] Q. Wen, W. Zhou, Y. Wang, Y. Qing, F. Luo, D. Zhu, Z. Huang, J. Mater Sci. 52, 832-842 (2017).

Figures

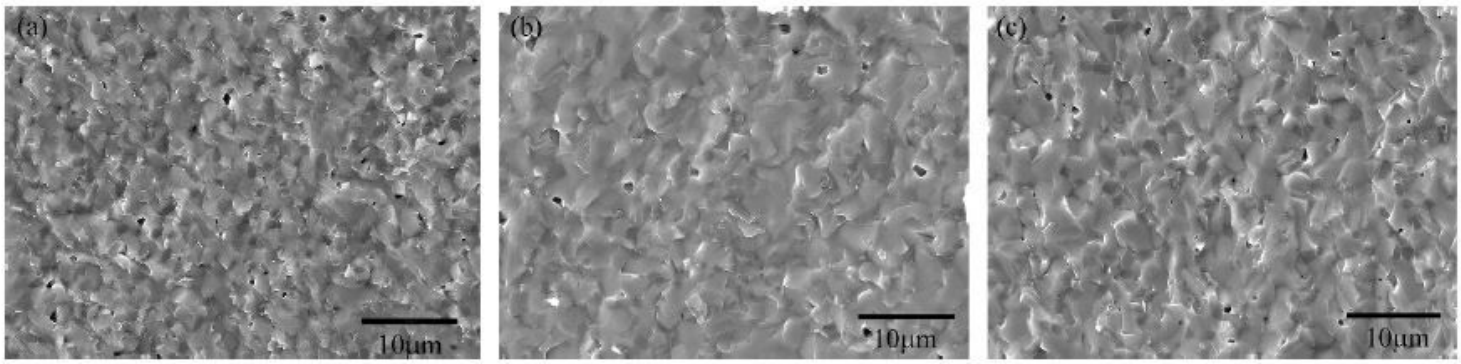

Figure 1

SEM images of the fracture cross-section morphologies of TiO2-Sr1-xLaxTiO3: (a) x=0.1, (b) x=0.2, (c) x=0.3.

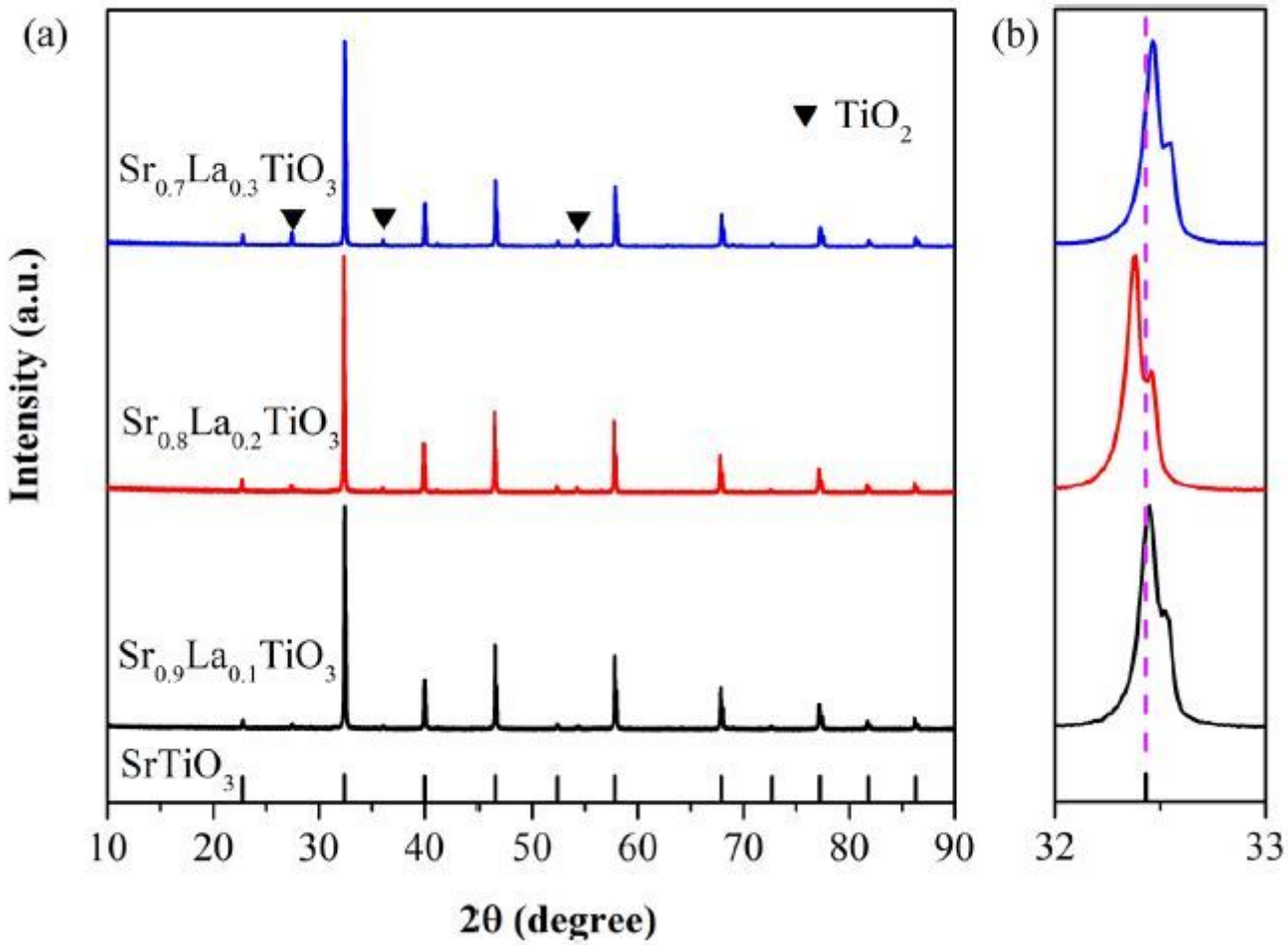

Figure 2

XRD diffraction patterns of TiO2-Sr1-xLaxTiO3: (a) whole patterns; (b) magnification peak distributed from 32° to 33°.

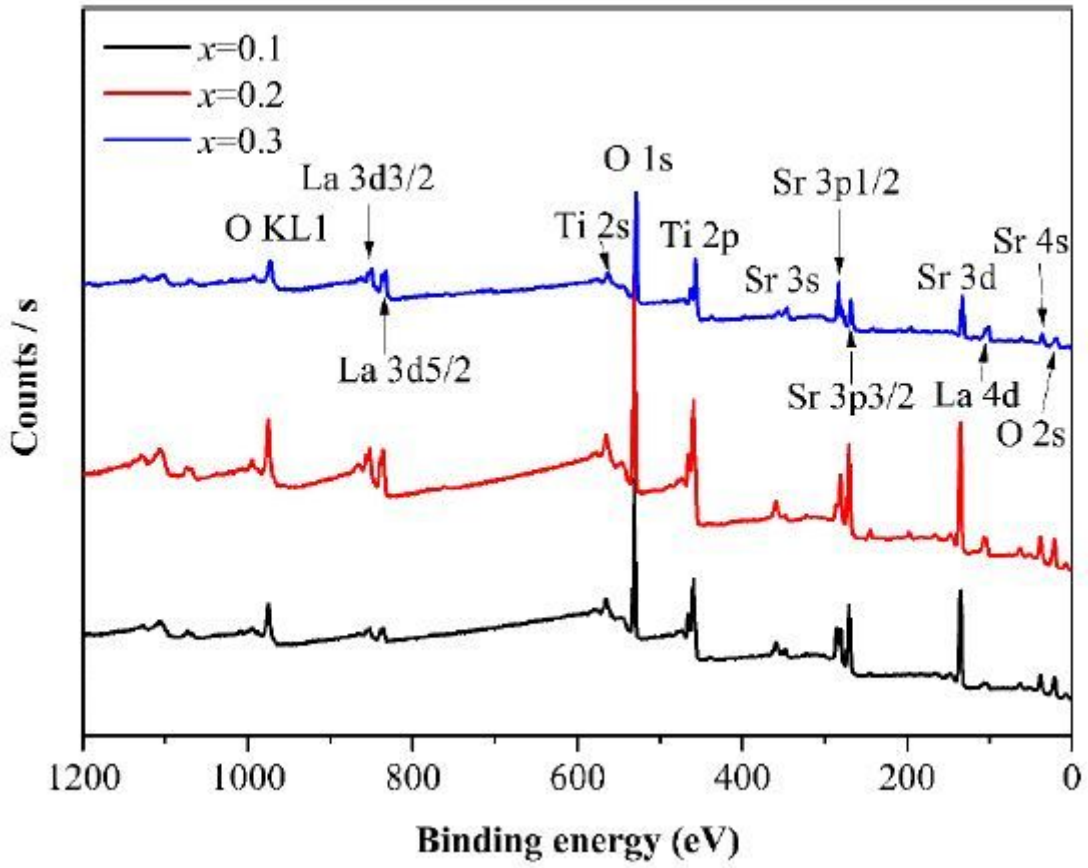

Figure 3

A wide survey scan XPS spectra of TiO2-Sr1-xLaxTiO3.

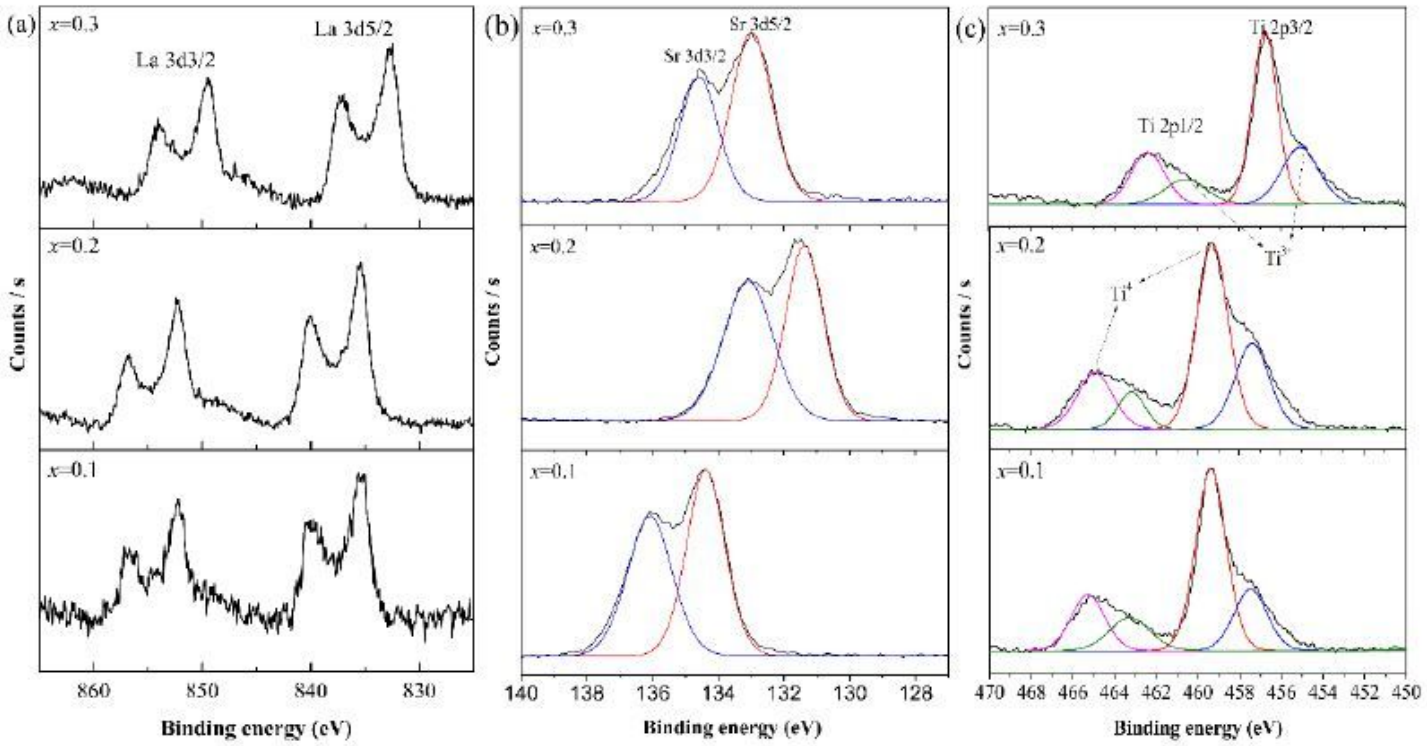

Figure 4

High-resolution XPS spectra of TiO2-Sr1-xLaxTiO3 ceramics in (a) La, (b) Sr and (c) Ti.

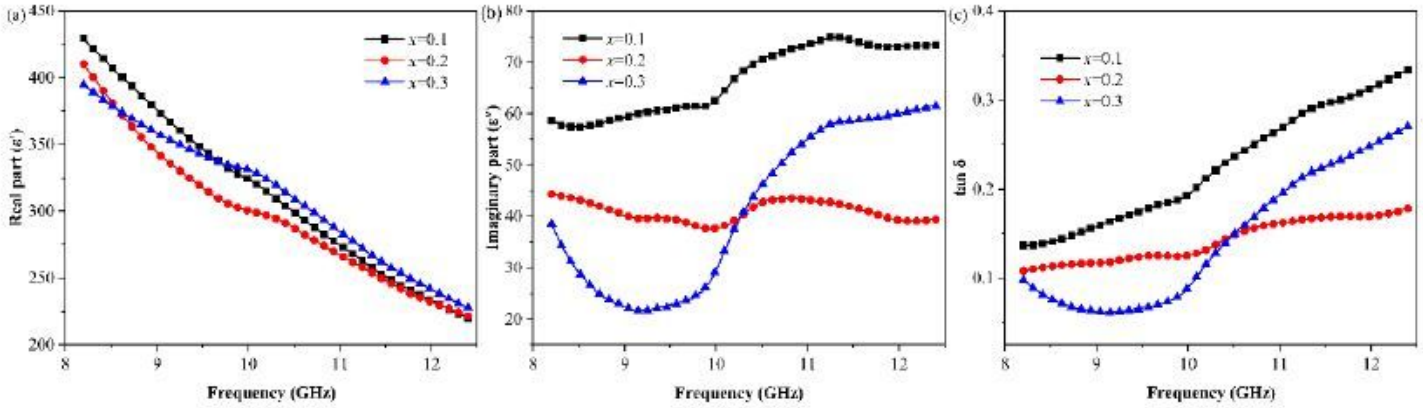

Figure 5

Dielectric parameters of (a) the real part, (b) the imaginary part, and (c) the dielectric loss for TiO2-Sr1-xLaxTiO3 ceramics.

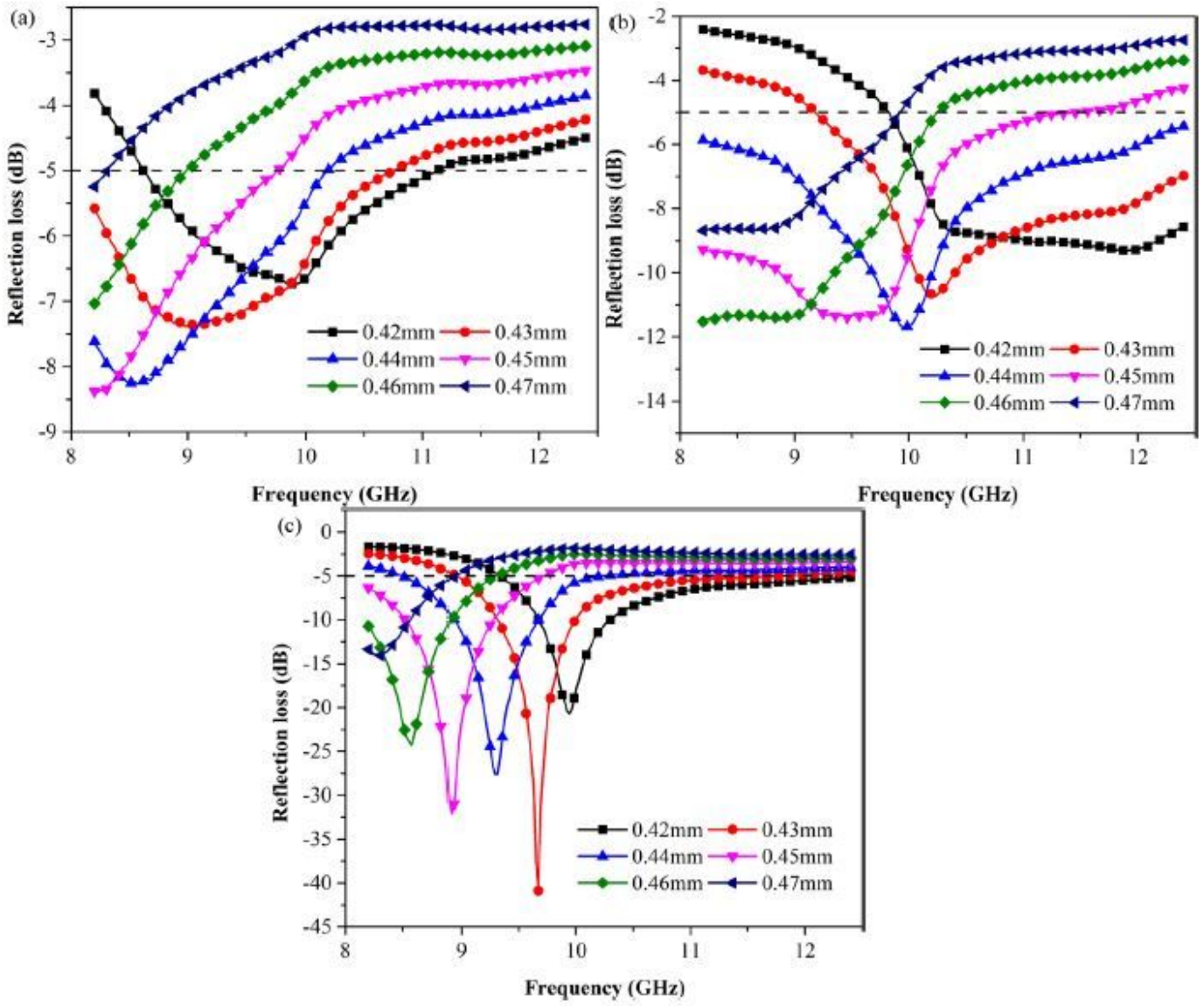

Figure 6

Reflection loss of (a) TiO2-Sr0.9La0.1TiO3, (b) TiO2-Sr0.8La0.2TiO3, and (c) TiO2-Sr0.7La0.3TiO3 with different thicknesses.

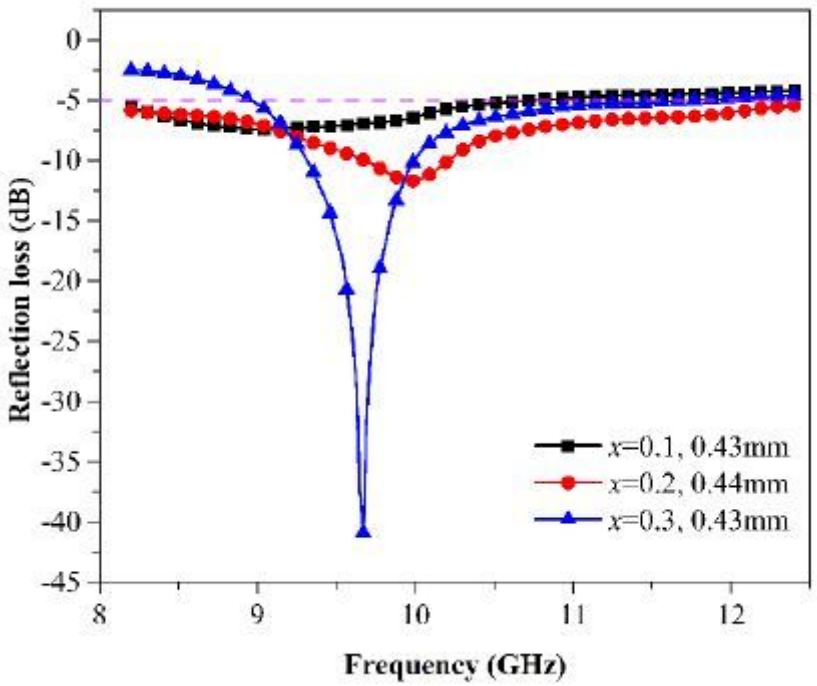

Figure 7

Comparison of reflection loss value of TiO2-Sr1-xLaxTiO3 (x=0.1~0.3) ceramics with optimum thicknesses.

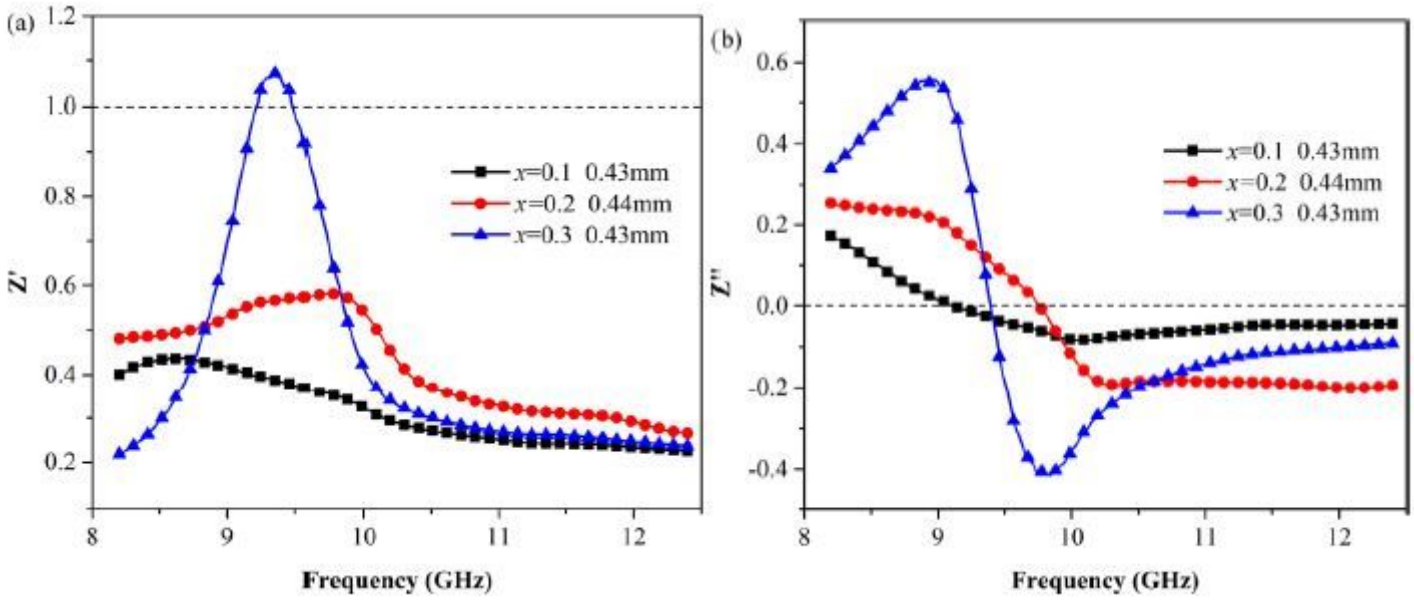

Figure 8

Plots of (a) real and (b) imaginary parts of impedance of TiO2-Sr1-xLaxTiO3 with optimum thicknesses.